Eur. Phys. J. D **38**, 231–236 (2006)
DOI: 10.1140/epjd/e2006-00001-y

THE EUROPEAN PHYSICAL JOURNAL D

State-selection and orientation of CH radicals by an electric hexapole

H. Ohoyama[a], Y. Nagamachi, and T. Kasai

Department of Chemistry, Graduate School of Science, Osaka University, Toyonaka, Osaka 560-0043, Japan

Received 1st August 2005 / Received in final form 18 November 2005
Published online 10 January 2006

Abstract. A pure and high intense pulsed supersonic CH ($X^2\Pi$) radical beam source was developed via the $C(^1D)$ + H_2 reaction. An electrostatic hexapole field was used to state-select CH radicals. The focusing curves for the single rotational states of CH were measured for the first time by a saturated laser-induced fluorescence (SLIF) spectroscopy for the R-branch in $A^2\Delta_{3/2} \leftarrow X^2\Pi_{1/2}$ transition. The focusing curves were simulated by the classical trajectory simulation based on a Stark energy analysis of the rotational energy levels, including spin-orbit and Λ-doubling coupling effects. In addition, orientational distribution functions were calculated for the selectable states.

PACS. 39.10.+j Atomic and molecular beam sources and techniques

1 Introduction

CH radical is one of the most important radicals as an intermediate in various reactions, such as hydrocarbon combustion [1] and planetary atmosphere [2]. From theoretical and practical importance of CH reactions, it is worthwhile to develop a high-intensity, high purity state-selected CH radical beam source for advanced experimental studies in gas phase and surface molecular reaction dynamics. However, the formation of CH radical with high intense and high purity is one of the most difficult subjects, because the process of CH radical generation simultaneously generates the mixture of other reactive species. From this reason, the studies on it's reaction dynamics have been extremely limited.

Recently, the hexapole technique has been applied to focus reactive radicals produced in a plasma discharge beam source [3–7]. The combination of a rotationally cold supersonic beam and a long hexapole field has achieved essentially pure rotational state-selection. Even in such case, however, pure rotational state-selection was useful only for a few lowest states. For CH radicals, Curtiss et al. have measured the CH focusing curve provided by a continuous discharge source using a quadrupole mass spectrometry [3]. Their focusing curve was obtained as the difference signal corrected by an appropriate subtraction of large background signal that comes from the fragmentation of the focusable C_2H radical. The focusing curve could not be state-resolved and had no clear structure. In addition, the agreement with the simulation appears to not good enough to allow the identification of each rotational state. As can be seen in this case, practically, the orientational selection is mostly carried out as an ensemble average of orientational states. From this reason, the simulation of the focusing curve is very important to know the rotational state distribution of the state ensemble after the hexapole state-selection.

More recently, we succeeded in developing a high-intense and highly purified CH radical beam source [8,9]. In the previous study, the CH beam source was characterized by a saturated laser-induced fluorescence spectroscopy (SLIF). The selection and purification of CH by the hexapole focusing from the byproducts was satisfactorily accomplished.

In the present study, the focusing curves for the single rotational states of CH were measured for the first time by using a saturated laser-induced fluorescence (SLIF) spectroscopy for the R-branch in $A^2\Delta_{3/2} \leftarrow X^2\Pi_{1/2}$ transition [10,11]. The state-resolved focusing curves enable us to make a reliable comparison with trajectory simulation of individual rotational states. In other word, the influence of Λ-doubling coupling effect upon hexapole state-selection of CH can be directly examined by the classical trajectory simulation based on a Stark energy analysis of the rotational energy levels, including spin-orbit and Λ-doubling coupling effects. In the present study, such a classical trajectory simulations were also carried out, and the results were compared with the experimental ones. The trajectory simulations were in good agreement with the experimental results. It was confirmed that Λ-doubling coupling effects give a significant effect for the CH focusing.

[a] e-mail: ohyama@chem.sci.osaka-u.ac.jp

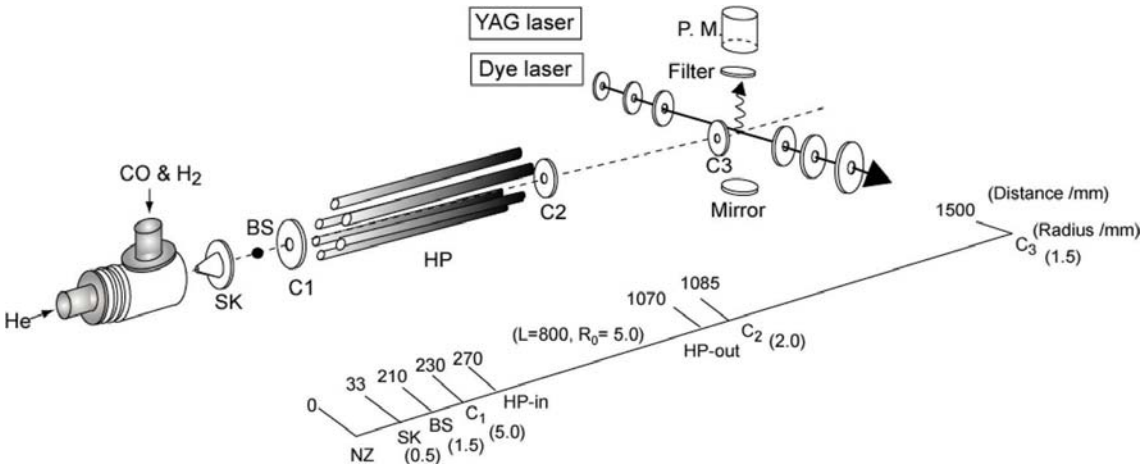

Fig. 1. A schematic view of the experimental apparatus for measuring the focusing curve of each single rotational state. NZ: Nozzle, SK: skimmer, BS: beam stop, C_1, C_2, C_3: collimators whose sizes and the distances form the nozzle were shown in the figure, HP: 80-cm long hexapole field constructed by 6 mm ϕ rods that were mounted with $R_0 = 5$ mm, P.M.: photomultiplier.

For the application of oriented CH beam to the study on steric effect, it is required to know the orientational distribution of CH beam. For this purpose, the orientational distribution functions were calculated for the selectable states.

2 Experimental

2.1 Focusing curve of state-selected CH

A schematic view of the experimental apparatus was shown in Figure 1. The detail of the CH source has been reported elsewhere [8]. Briefly, CH was generated from the following reaction scheme:

$$\begin{aligned}
&\mathrm{He} \rightarrow \mathrm{He}^*(2^3\mathrm{S}),\\
&\mathrm{He}^*(2^3\mathrm{S}) + \mathrm{CO}(\mathrm{X}^1\Sigma^+) \rightarrow \mathrm{C}(^1\mathrm{D}) + \mathrm{O} + \mathrm{He},\\
&\mathrm{C}(^1\mathrm{D}) + \mathrm{H_2} \rightarrow \mathrm{CH}(\mathrm{X}^2\Pi, v = 0).
\end{aligned}$$

$\mathrm{He}^*(2^3\mathrm{S})$ was generated by a pulsed DC discharge and entered into a channel reactor filled with the (1:1) premixed gas of $\mathrm{H_2/CO}$. The $\mathrm{H_2/CO}$(1:1) and He gas were injected from the pulsed valve at the stagnation pressure of 140 and 1800 Torr, respectively. The CH radicals were state-selected and focused into the point 150 cm downstream from nozzle by an 80 cm-long electrostatic hexapole field. The focusing curves for each $|J, Fi, M\rangle$ rotational state of CH were measured by the saturated laser-induced fluorescence (SLIF) method for R-branch in $\mathrm{A}^2\Delta_{3/2} \leftarrow \mathrm{X}^2\Pi_{1/2}$ transition. The 430-nm probe light is the light from dye laser operated with Stillben 420 pumped by YAG laser. The LIF signal was detected by a photomultiplier (Hamamatsu R1635P) mounted at 7 cm apart from the beam crossing point and counted by a photon-counter (Stanford SR400). The gate width was set to 1.0 μs with the delay time of 20 ns after the laser irradiation.

2.2 Trajectory simulation for focusing of CH radical

For Hund's case (a), the rotational wave function of the diatomic molecules in the $^2\Pi$ state is generally characterized by the total angular momentum quantum number J, its projection M on the space-fixed axis, and its projection $\Omega = \Lambda + \Sigma$ on the molecular axis. The wave function is given by [12]

$$\phi_\varepsilon(\Omega, J, M) = 1/\sqrt{2}\,(|\Omega, J, M\rangle + \varepsilon\,|-\Omega, J, M\rangle) \qquad (1)$$

where $\varepsilon = \pm 1$ denotes the parity index quantum number. The parity depends also on the value of quantum number J. The state with $\varepsilon = +1$ has the e-symmetry and the state with $\varepsilon = -1$ is the f-symmetry.

For the intermediate case of Hund's case (a) and (b) that CH radical belongs to, the field free wave functions are given by [13,14]

$$\begin{aligned}
\Phi_{\varepsilon,Fi}(J, M) = a_{Fi,J}\phi_\varepsilon(\Omega = 1/2, J, M)\\
+ b_{Fi,J}\phi_\varepsilon(\Omega = 3/2, J, M)
\end{aligned} \qquad (2)$$

where Fi denotes the fine structure state.

The coefficients $a_{Fi,J}$ and $b_{Fi,J}$ are described [12]:

$$a_{1,J} = b_{2,J} = [(X + Y - 2)/2X]^{1/2} \qquad (3a)$$

$$b_{1,J} = -a_{2,J} = [(X - Y + 2)/2X]^{1/2} \qquad (3b)$$

where

$$X = \left[4(J + 1/2)^2 + Y(Y - 4)\right]^{1/2} \qquad (4a)$$

$$Y = A/B \qquad (4b)$$

A is spin-orbit constant, B is rotational constant, and J is the rotational quantum number.

The rotational energy levels for doubly degenerate parity pair were given originally by Hill and van Vleck as follows [15]:

$$E(J) = B[(J - 1/2)(J + 3/2) \pm (1/2)X].$$

The energy levels associated with the plus sign are called F_2, $Fi = 2$; those with the minus sign F_1, $Fi = 1$. F_1 is the term series that forms levels with $J = N + 1/2$, and F_2 forms levels with $J = N-1/2$ (N means $J = N+S$, angular momentum excluding spin).

In the electric field E, the e-symmetry state $\Phi_{+1,Fi}(J,M)$ and the f-symmetry state $\Phi_{-1,Fi}(J,M)$ are coupled. The coupling matrix element of $\vec{\mu}\cdot\vec{E}$, W_{stark} is expressed as

$$\begin{aligned} W_{stark} &= \langle \Phi_{\pm 1,Fi}(J,M)\,|-\mu E|\,\Phi_{\mp 1,Fi}(J,M)\rangle \\ &= -\mu E \frac{M}{J(J+1)}\left[1/2(a_{Fi,J})^2 + 3/2(b_{Fi,J})^2\right] \\ &\equiv -\mu E \frac{M\Omega_{eff}}{J(J+1)} \equiv -\mu_{eff} E \end{aligned}$$

where μ is the permanent dipole moment of CH; $\mu = 1.46$ D [16]. By using the values of $A = 28.1467$ cm^{-1} and $B = 14.1923$ cm^{-1} [17], the simple relationship of $a^2_{Fi,J} \approx b^2_{Fi,J} \approx 1/2$ is found to hold for the CH radical except for the $|J, Fi\rangle = |1/2, 2\rangle$ state that has $a^2_{Fi,J} = 1$ and $b^2_{Fi,J} = 0$. As a result, the value of Ω_{eff} becomes $1/2$ for the $|J, Fi\rangle = |1/2, 2\rangle$ state and almost unity for the other rotational states. This could mean that one is not able to separate F_1 state from F_2 state at the same $J > 1/2$ and $M = J$ except due to a difference in Λ-doubling between these two manifolds.

The shift and splitting in energy due to Stark effect is then given by the eigenvalues of the 2×2 matrix

$$\begin{vmatrix} W_\Lambda - W_\varepsilon & W_{stark} \\ W_{stark} & -W_\varepsilon \end{vmatrix} = 0$$

where W_Λ denotes the Λ-doubling splitting between the doublet states in zero field. Strictly speaking, we must include the magnetic hyperfine interaction in the calculation, because the H of CH carries a nuclear spin $I = 1/2$, which couples in a low external field situation to J always as $F = J + I$. However, we omit this effect in the further calculation, because the hyperfine interaction in CH is rather small [11].

Diagonalization of this matrix gives the eigenvalues [13,14,18]:

$$W_{\pm 1}(E) = (1/2)W_\Lambda \left(1 \pm \sqrt{1 + \left(\frac{2\mu_{eff}E}{W_\Lambda}\right)^2}\right).$$

This leads to the radial force of CH in an ideal hexapole field:

$$\begin{aligned} F_r &= -\frac{\partial W \pm (E)}{\partial r} = -\frac{\partial W_\pm(E)}{\partial E}\frac{\partial E}{\partial r} \\ &= \mp\left[\frac{W_\Lambda^2}{4} + \mu_{eff}^2 \frac{9V_0^2 r^4}{R_0^6}\right]^{-1/2} \mu_{eff}^2 \frac{18V_0^2}{R_0^6} r^3 \end{aligned}$$

where V_0 is the hexapole voltage, R_0 is the radial distance of the hexapole face from the central axis of the hexapole, r is the radial coordinate. This radial force was applied in the trajectory simulation of the focusing behavior of CH in the hexapole field. In the simulation, an exact numerical calculation of the molecular motion in the hexapole field was carried out point-by-point following Newton's equation. The CH motion was calculated for the set of two parameters of v and ϕ. Where, v is the incident velocity, ϕ is the incident angle that is defined as the angle between the incident velocity and the hexapole central axis. The statistical weight of these parameters was calculated from the velocity distribution and the distribution of the incident angle determined by the solid angle restricted by the geometrical parameters. The velocity distribution was measured by a conventional time-of-flight method. It was characterized by the shifted-Maxwellian distribution using two parameters, v_s and α_s [19]. The parameters were determined to be $v_s = 1650$ ms^{-1} and $\alpha_s = 350$ ms^{-1}. The geometrical factors are the hexapole radius and length as well as the collimator sizes and their locations with respect to the beam source and detector. They are summarized in Figure 1. A point source at the nozzle is assumed as the starting point of every trajectory. The detail of the simulation process has been described in the previous paper [20].

2.3 Orientational distribution of CH in an electric field

Diagonalization of the above 2×2 matrix give the field dependent eigenfunctions that can be expressed as the linear combination of the field free eigenfunctions [13,14]:

$$\begin{aligned} \Psi_{\varepsilon,Fi}(E,J,M) = \alpha_{\varepsilon,Fi}(E)\Phi_{-1,Fi}(J,M) \\ + \beta_{\varepsilon,Fi}(E)\Phi_{+1,Fi}(J,M) \end{aligned} \quad (5)$$

where

$$\alpha^2_{\mp 1,Fi}(E) = \beta^2_{\pm 1,Fi}(E) = \frac{1}{2} \pm \frac{1}{2\sqrt{1 + \left(\frac{2\mu_{eff}E}{W_\Lambda}\right)^2}}.$$

Using the field dependent eigenfunction, the orientational distribution function for each rotational eigenstate is described as

$$\begin{aligned} P^\varepsilon_{Fi,J,M}(E,\cos\theta) &= \iint \Psi^*_{\varepsilon,Fi}(E,J,M)\Psi_{\varepsilon,Fi}(E,J,M)d\varphi d\psi \\ &= \left[\frac{(\alpha_{\varepsilon,Fi} + \beta_{\varepsilon,Fi})}{\sqrt{2}} a_{Fi,J}\right]^2 |\phi(\Omega = 1/2, J, M)|^2 \\ &+ \left[\frac{(\alpha_{\varepsilon,Fi} - \beta_{\varepsilon,Fi})}{\sqrt{2}} a_{Fi,J}\right]^2 |\phi(\Omega = -1/2, J, M)|^2 \\ &+ \left[\frac{(\alpha_{\varepsilon,Fi} + \beta_{\varepsilon,Fi})}{\sqrt{2}} b_{Fi,J}\right]^2 |\phi(\Omega = 3/2, J, M)|^2 \\ &+ \left[\frac{(\alpha_{\varepsilon,Fi} - \beta_{\varepsilon,Fi})}{\sqrt{2}} b_{Fi,J}\right]^2 |\phi(\Omega = -3/2, J, M)|^2. \end{aligned} \quad (6a)$$

For the each $|\phi(\Omega,J,M)|^2$, the function can be expanded by a series of Legendre polynomials as

$$|\phi(\Omega,J,M)|^2 = \frac{2J+1}{2}\sum_{n=0}^{2J} C_n(\Omega,J,M)P_n(\cos\theta).$$

The coefficient C_n is written as [21]

$$C_n(\Omega,J,M)=(2n+1)(-1)^{M-\Omega}\begin{pmatrix} J & J & n \\ \Omega & -\Omega & 0\end{pmatrix}\begin{pmatrix} J & J & n \\ M & -M & 0\end{pmatrix}.$$

Finally, for each rotational eigenstate in the electric field, the expansion coefficients of the orientational distribution function, $P^{\varepsilon}_{Fi,J,M}(E,\cos\theta)$, by Legendre polynomials is expressed as follows

$$\begin{aligned} C_n(\varepsilon,Fi,E,J,M) = & \left[\frac{(\alpha_{\varepsilon,Fi}+\beta_{\varepsilon,Fi})}{\sqrt{2}}a_{Fi,J}\right]^2 C_n\left(\Omega=1/2,J,M\right) \\ & + \left[\frac{(\alpha_{\varepsilon,Fi}-\beta_{\varepsilon,Fi})}{\sqrt{2}}a_{Fi,J}\right]^2 C_n\left(\Omega=-1/2,J,M\right) \\ & + \left[\frac{(\alpha_{\varepsilon,Fi}+\beta_{\varepsilon,Fi})}{\sqrt{2}}b_{Fi,J}\right]^2 C_n\left(\Omega=3/2,J,M\right) \\ & + \left[\frac{(\alpha_{\varepsilon,Fi}-\beta_{\varepsilon,Fi})}{\sqrt{2}}b_{Fi,J}\right]^2 C_n\left(\Omega=-3/2,J,M\right). \end{aligned} \quad (6b)$$

This result was used for the calculation of the orientational distribution for each $|J,Fi,M\rangle$ state as the function of the electric field strength.

3 Results and discussion

3.1 Focusing of CH by a hexapole field

Figure 2A shows the focusing curve for the single rotational state of $|J,Fi,M\rangle = |1/2,2,1/2\rangle$ measured by the saturated laser-induced fluorescence (SLIF) method for R-branch in $A^2\Delta_{3/2} \leftarrow X^2\Pi_{1/2}$ transition without beam stop. This is the focusing curve measured for a single state-selected CH beam for the first time. The focusing curve showed a distinctive feature of long asymmetric tail to higher voltage. The simulated focusing curve including Λ-doubling coupling effect was shown in Figure 2A as a solid line. The coefficients, $a_{Fi,J}$ and $b_{Fi,J}$ calculated from equations (3a) and (3b) were shown in the figure. As a reference, the simulated focusing curve without Λ-doubling coupling effect was shown in the same figure as a dashed line. The calculated focusing curve including no Λ-doubling coupling effect (dashed line) had no such asymmetric feature. While, the simulation including Λ-doubling coupling effect (solid line) showed the asymmetric feature and was in good agreement with the experimental result. From the comparison of two calculated focusing curves with the experimental one, it was found that the asymmetric feature is due to the Λ-doubling coupling effect. In addition, it was confirmed that Λ-doubling coupling effect gives the significant effects for the CH focusing: the shift of the peak position and the broadening of the state-selection.

For the application of the state-selected CH beam, it is very important to achieve a good resolution of the state-selection. A beam stop is expected to be efficient to improve the state resolution in the focused beam, because the beam stop selectively removes the trajectories that are more affected by the Λ-doubling coupling effect in the weaker electric field near the central axis of the hexapole. To make sure this point, the focusing curve for the $|J,Fi,M\rangle = |1/2,2,1/2\rangle$ rotational state was measured with beam. Figure 2B shows the focusing curve measured with beam stop. At a glance, it is found that the asymmetric feature of the focusing curve due to the Λ-doubling coupling effect is clearly disappeared. The resolution of the focusing curve was greatly improved as compared with the one without beam stop. Figure 3 shows the focusing curves measured for each $|J,Fi\rangle$ rotational state of CH with beam stop. In all cases, there were no asymmetric features in the focusing curves. It was confirmed that the beam stop is very useful to improve the state resolution of the focusing curve of CH. The simulated focusing curves including spin-orbit and Λ-doubling coupling effects were shown in Figure 3 as the solid lines. As a reference, the coefficients, $a_{Fi,J}$ and $b_{Fi,J}$ calculated from equations (3a) and (3b) were shown in the figures. The simulated focusing curves without Λ-doubling coupling effects were also shown in the same figure as the dashed lines.

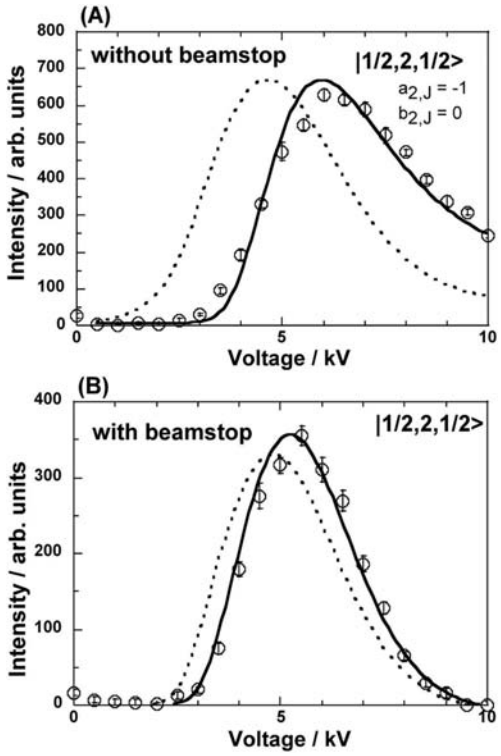

Fig. 2. Open circles: focusing curve for the $|J,Fi,M\rangle = |1/2,2,1/2\rangle$ rotational state of CH measured by the saturated laser-induced fluorescence (SLIF) method for R-branch in $A^2\Delta_{3/2} \leftarrow X^2\Pi_{1/2}$ transition: (A) without beam stop, (B) with beam stop; solid lines: focusing curves simulated including Λ-doubling coupling effect; dashed lines: focusing curves simulated without Λ-doubling coupling effect. The coefficients, $a_{Fi,J}$ and $b_{Fi,J}$ calculated from equations (3a) and (3b) were shown.

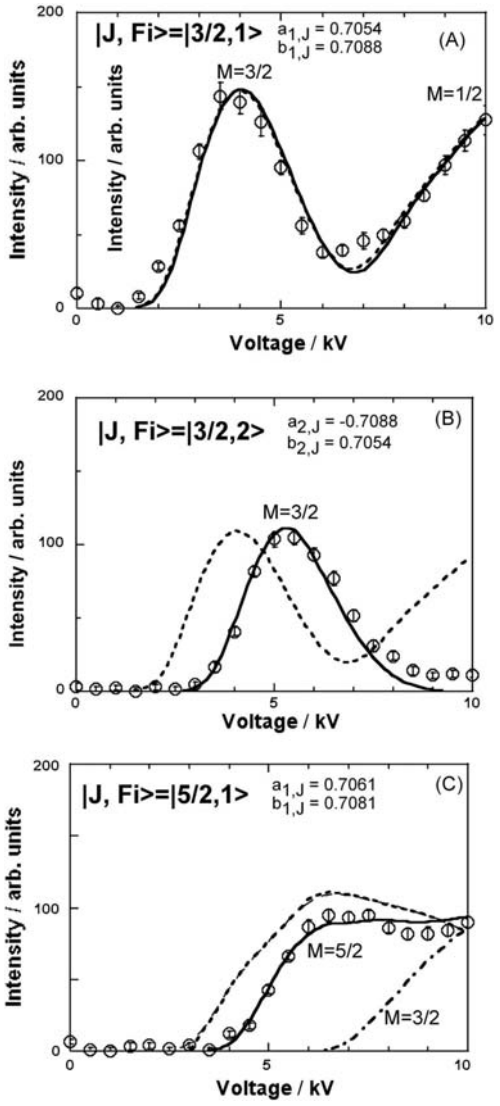

Fig. 3. Open circles: focusing curves for each $|J, Fi\rangle$ rotational state of CH with beam stop measured by the saturated laser-induced fluorescence (SLIF) method for R-branch in $A^2\Delta_{3/2} \leftarrow X^2\Pi_{1/2}$ transition: (A) $|3/2, 1\rangle$, (B) $|3/2, 2\rangle$, (C) $|5/2, 1\rangle$; solid lines: focusing curves simulated including spin-orbit and Λ-doubling coupling effects; dashed lines: focusing curves simulated without Λ-doubling coupling effect. The coefficients, $a_{Fi,J}$ and $b_{Fi,J}$ calculated from equations (3a) and (3b) were shown for each $|J, Fi\rangle$ rotational state. The contribution of $|J, Fi, M\rangle = |5/2, 1, 3/2\rangle$ state in the focusing curve (C) is shown as a dotted-dashed line.

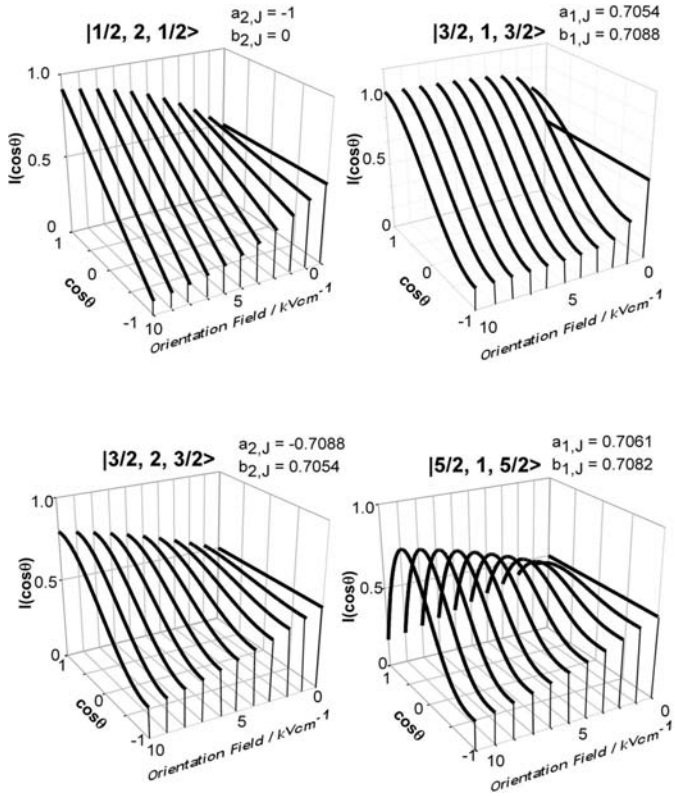

Fig. 4. Orientational distributions of CH for each single-rotational $|J, Fi, M\rangle$ state in the electric field. The coefficiencies, $a_{Fi,J}$ and $b_{Fi,J}$ calculated from equations (3a) and (3b) were shown for each $|J, Fi, M\rangle$ rotational state.

For the $|J, Fi\rangle = |3/2, 1\rangle$ state that has small Λ-doubling splitting of 725 MHz [22], both simulations nicely reproduced the experimental one. While, for the other states that have large Λ-doubling splitting, it was found that only the simulation based on a Stark energy analysis of the rotational energy levels, including spin-orbit and Λ-doubling coupling effects can nicely reproduce the experimental ones. Especially, large peak shift was recognized for the $|J, Fi\rangle = |3/2, 2\rangle$ state that has large Λ-doubling splitting of 7325 MHz [23]. It was confirmed that Λ-doubling coupling effects give a significant peak shift for the CH focusing with beam stop. For the $|J, Fi\rangle = |5/2, 1\rangle$ state, the single state selection of $|J, Fi, M\rangle$ state is found to be difficult. The contribution of $|J, Fi, M\rangle = |5/2, 1, 3/2\rangle$ state in the focusing curve is shown as a dotted-dashed line.

3.2 Orientational distribution of CH in an electric field

The calculated orientational distributions for each single-rotational state were shown in Figure 4 as the function of the orientation field-strength. It was found that the dependences of the orientational distributions on the orientation field-strength are dramatically changed depending on the rotational state. The significant Λ-doubling coupling effect was recognized for the CH orientation. The theoretical calculations show that the orientation field strength of 3 $\mathrm{kV\,cm^{-1}}$ is enough to get good orientation for $|J, Fi, M\rangle = |3/2, 1, 3/2\rangle$ state that has small Λ-doubling splitting of 725 MHz. While, the orientation field strength higher than 10 $\mathrm{kV\,cm^{-1}}$ is necessary for the $|J, Fi, M\rangle = |1/2, 2, 1/2\rangle$, $|3/2, 2, 3/2\rangle$ and $|5/2, 1, 5/2\rangle$ states, because of their large Λ-doubling splitting, 3263, 7274, 4847 MHz respectively [23]. These calculated results are applying for the study on stereodynamics for the CH + NO reaction. The results will be shown in elsewhere [24].

References

1. W.A. Sanders, M.C. Lin, *Chemical Kinetic of Small Organic Radicals*, edited by Z.B. Alfassi (CRC, Boca Raton, FL, 1986), Vol. III
2. M. Lindqvist, A. Sandqvist, A. Winnberg, L. Johansson, L.-A. Nyman, Astron. Astrophys. Suppl. Ser. **113**, 257 (1995)
3. M.A. Weibel, T.D. Hain, T.J. Curtiss, J. Chem. Phys. **108**, 3134 (1998)
4. T.D. Hain, M.A. Weibel, K.M. Backstran, T.J. Curtiss, J. Phys. Chem. A **101**, 7674 (1997)
5. K. Schreel, J.J. ter Meulen, J. Phys. Chem. A **101**, 7639 (1997)
6. K. Ikejiri, H. Ohoyama, Y. Nagamachi, T. Teramoto, T. Kasai, Chem. Phys. Lett. **379**, 255 (2003)
7. M. Takezaki, H. Ohoyama, T. Kasai, K. Kuwata, Laser Chem. **15**, 113 (1994)
8. K. Ikejiri, H. Ohoyama, Y. Nagamachi, T. Kasai, Chem. Phys. Lett. **401**, 465 (2005)
9. Y. Nagamachi, H. Ohoyama, K. Ikejiri, T. Kasai, J. Chem. Phys. **122**, 064307 (2005)
10. C.R. Brazier, J.M. Brown, Can. J. Phys. **62**, 1563 (1984)
11. M. Zachwieja, J. Mol. Spectrosc. **170**, 285 (1995)
12. R.N. Zare, *Angular Momentum* (Wiley, New York, 1998)
13. K. Schreel, J.J. ter Meulen, J. Phys. Chem. A **101**, 7639 (1997)
14. T.D. Hain, M.A. Weibel, K.M. Backstrand, T.J. Curtiss, J. Phys. Chem. A **101**, 7674 (1997)
15. E.L. Hill, J.H. van Vleck, Phys. Rev. **32**, 250 (1923)
16. D.R. Lide, *CRC Handbook of Chemistry and Physics*, 74th edn. (CRC, Boca Raton, FL, 1993), Section 9
17. M. Zachwieja, J. Mol. Spectrosc. **70**, 285 (1995)
18. M.G. Tenner, E.W. Kuipers, W.Y. Langhout, A.W. Kleyn, S. Stolte, Surf. Sci. **236**, 151 (1990)
19. R.B. Bernstein, *Chemical Dynamics via Molecular Beam and Laser Techniques* (Oxford University Press, New York, 1982), Chap. 3
20. H. Ohoyama, T. Ogawa, T. Kasai, J. Phys. Chem. **99**, 13606 (1995)
21. S. Stolte, Ber. Bunsenges. Phys. Chem. **86**, 413 (1982)
22. L.M. Ziutys, B.E. Turner, Astrophys. J. **292**, L25 (1985)
23. M. Goto, S. Saito, Astrophys. J. **452**, L147 (1995)
24. Y. Nagamachi, H. Ohoyama, T. Kasai (in preparation)